General and Simple Approach for Control Cage and Cylindrical Mesopores, and Thermal/Hydrothermal Stable Frameworks

Sherif A. El-Safty,* Fujio Mizukami, and Takaaki Hanaoka[#]

Laboratory for Membrane Chemistry, Tohoku Center, National Institute of Advanced Industrial Science and Technology (AIST), 4-2-1 Nigatake, Miyagino-ku, Sendai, 983-8551, Japan

Received: January 18, 2005; In Final Form: March 16, 2005

Highly ordered cage and cylindrical mesoporeous silica monoliths (HOM) with 2- and 3-dimensional (2D and 3D, respectively) structures, mesopore/micropore volumes, and thick-walled frameworks were successfully fabricated by instant direct templating of lyotropic phases of copolymer ($EO_m-PO_n-EO_m$) surfactants. Large cage-like pores with uniform constriction sizes up to 10 nm and open cylindrical channel-like mesopores can be easily achieved by this simple and efficient synthesis design. Our results show that the cage-like pores could be fabricated at relatively lower copolymer concentrations used in the lyotropic phase domains at copolymer/TMOS ratios of 35 wt %. These ordered cage pore architectures underwent transition to open-cylindrical pores by increasing the copolymer concentration. High EO/PO block copolymers, in general, were crucially affected on the increase of the interior cavity sizes and on the stability of the cage mesopore characters. However, for F108 ($EO_{141}PO_{44}EO_{141}$) systems, the fabrication of ordered and stable cage pore monoliths was achieved with significantly higher copolymer concentrations up to 90 wt %. Interestingly, the effective copolymer molecular nature was also observed in the ability to design various ordered mesophase geometries in large domain sizes. Our findings here show evidence that the synthetic strategy provides realistic control over a wide range of mesostructured phase geometries and their extended long-range ordering in the final replicas of the silica monolith frameworks. In addition, the HOM silica monoliths exhibited considerable structural stability against higher thermal temperature (up to 1000 °C) and longer hydrothermal treatment times under boiling water and steam. The remarkable structural findings of 3D frameworks, transparent monoliths, and micropores combined with large cage- and cylindrical-like mesopores are expected to find promising uses in materials chemistry.

Introduction

Hybrid organic−inorganic nanocomposite materials are of technological interest due to potential widespread applications.[1] A large variety of prospective surfactant-templated silica mesophases have been synthesized in the past decade.[2−9] A supramolecular templating mechanism is commonly accepted as being responsible for these hierarchically mesoporous materials.[10] The mesoporous synthetic strategy adopting the use of the triblock copolymers ($EO_mPO_nEO_m$) as templates in acidic conditions significantly enhanced the structural quality by cylindrical and cage pore frameworks, such as 2D hexagonal structures of SBA-15 with uniform cylindrical-like pore sizes up to 30 nm, by using P123 ($EO_{20}-PO_{70}-EO_{20}$) as a template.[7,11] Successful synthesis of cylindrical cubic *Ia*3*d* mesopores in the gyroid IPMS structure was also achieved by using P123 template in the presence of a high concentration of NaI (1 M)[12a] and butanol[12b] under strong acidic conditions.[14] Cage cubic *Im*3*m* and *Fm*3*m* structures of SBA-16 and KIT-5 with 5.4 and 6.8 nm dimensions were fabricated by using F127 ($EO_{106}-PO_{70}-EO_{106}$) as a template under high and low HCl concentrations, respectively.[11,13a] However, when the F127/trimethylbenzene (TMB) system was used as a template, ordered cubic structures (*Fm*3*m*, FDU-12) were fabricated that had large cage-like pores and entrance pore sizes in the 4−9 nm range.[13b] Synthesis involving copolymers of inorganic salts was used to fabricate large single crystals of *Im*3*m* (SBA-16-like) symmetry, using F108 ($EO_{132}-PO_{50}-EO_{132}$) as a template.[14] Moreover, triblock copolymer synthesis has been applied to produce periodically ordered non-silica mesoporous oxides in 2D *P*6*mm* hexagonal and cubic *Im*3*m* structures.[15] Although syntheses of these materials yielded ordered cage and cylindrical structures with large pore size up to 12 nm, the restrictive, time-consuming, and hydrothermal synthesis conditions used and the powdery products in small domain sizes could constrain their potentials. If these ordered 3D cage and cylindrical structures are fabricated by simple and reproducible synthesis designs into optically translucent monoliths that are crack-free in macroscopic length scale, then their applications can be widely expanded.[1,16]

The development of the tailoring and design strategies for the pore sizes of mesoporous materials has been actively researched because of the widespread applications of materials with controllable pore sizes.[17] Several approaches to enlarge the pore dimensions include the use of surfactants with different chain lengths,[7,11] use of a swelling agent (hydrocarbons and amines),[2,18] and use of high temperature during synthesis.[8] The retention of structural uniformity was sometimes degraded, however. For example, triblock copolymers $EO_mPO_nEO_m$ were swollen by TMB as a porogen to synthesize silica mesocellular foams (MCFs, and MSU-F) with uniform cell and large cylindrical-like pores in disordered structures that limit the applications.[19] Direct templating of microemulsion liquid crystal phases was also used to expand the mesopore sizes of ordered

* Address correspondence to this author. E-mail: sherif.el-safty@aist.go.jp.
[#] E-mail: hanaoka-takaaki@aist.go.jp.

10.1021/jp050304d CCC: $30.25
Published on Web 04/14/2005

TABLE 1: Structural Parameters[a] of Mesoporous Silica Cage (HOM-C) and Cylindrical (HOM-n) Monoliths Synthesized in Lyotropic Mesophases of Copolymers

mesophase synthesis conditions									
copolymer structures	copolymer/TMOS, wt %	T, °C	monolithic structure	V_P, cm^3/g	V_m, cm^3/g	α_0, Å	S_{BET}, m^2/g	R, Å	W, Å
P123 ($EO_{20}PO_{70}EO_{20}$)	35	45	(HOM-C1) *Im*3*m*	0.55	0.07	125	523	54	71
	50	40	(HOM-2) *P*6*mm*	1.0	0.06	102	700	72	30
	80	45	(HOM-5) *Ia*3*d*	1.05	0.04	215	583	78	137
	90	45		1.09	0.06	270	545	100	170
PF68 ($EO_{80}PO_{27}EO_{80}$)	50	45	(HOM-C5) *Ia*3*d*	0.92	0.05	188	790	54	134
	70	45		1.2	0.07	190	810	62	128
	80	45	(HOM-12) *Fm*3*m*−*I*	1.2	0.06	161	675	78	83
	90	45	(HOM-10) *Fm*3*m*	1.95	0.07	164	1150	78	86
F108 ($EO_{141}PO_{44}EO_{141}$)	35	50	(HOM-C1) *Im*3*m*	0.73	0.13	156	700	54	102
	50	50		0.77	0.16	157	784	68	89
	70	50		1.35	0.13	167	866	91	76
	80	50		1.9	0.12	178	996	100	78
	90	50	(HOM-C10) *Fm*3*m*	1.4	0.14	230	692	100	130

[a] Mesopore (V_p)/micropore (V_m) volumes, unit lattice dimension (α_o), BET surface area (S_{BET}), pore size (R), and wall thickness (W).

silica monoliths fabricated from block copolymer−water solutions mixed with alcohol cosurfactant and hydrophobic swelling agents, such as long chain alkanes or cyclohexane; however, the TMB had ineffective control over the pore structures of the monolithic phases.[20] Recently, significant attention also has been devoted to using block copolymer templates to control the sizes of the cavities and entrances of cubic *Fm*3*m* (FDU-1, 2) cage-like pores.[8b,13,21] The use of block copolymer/cationic surfactant mixtures as templates enables formation of hexagonal structures, such as SBA-15 with cage-like pores (PSU-1).[22]

One of the most outstanding challenges in the design of such periodic mesoporous composites (monoliths and powder forms) is improving their thermal/hydrothermal stabilities; due to the amorphous atomic scale of the network pores, however, the periodic order structures might collapse under hydrothermal treatments such as boiling and steaming. This tendency for structural collapse under such hydrothermal treatment has diminished their functionality, particularly in industrial applications. Significant effort has been devoted to increase the mesostructured stability such as doping of heteroatoms, coating by zeolite-like species, which protect the silica frameworks, or introduction of stable structural unites into the wall architectures,[23] suggesting that the synthesis treatment significantly influenced crucial governing factors in the framework cross-linking and the thicker structural walls to provide the actual structural stability.[23] Although these development efforts have led to increased hydrothermal stability of the resultant materials, the complexity of the stabilization procedures that diminished mesoporous structural periodicity and properties could constrain the facile and commercial applications of these materials in the petrochemical industry.

In this study, we developed a strategy for fabricating ordered, translucent, crack-free, and shape-controlled 2D and 3D mesoporous silica monoliths by using lyotropic liquid crystal phases of selected copolymers (Pluronic-types) as templates. The methodology involved simple, rapid (within minutes) phase geometrical control, and thus yielded enriched surfactant phases, thick framework walls, and adjustable sizes of the entrances to large-cage pores and open-ended cylindrical-like pores. In these synthetic systems, the copolymer concentrations and the copolymer molecular natures crucially affected the mesophase structural changes and pore-size enlargement. In general, the following HOM silica monoliths were successfully fabricated: HOM-2 (2D hexagonal *P*6*mm*, SBA-15-like), HOM-1 (cubic *Im*3*m* with IWP-like morphology), HOM-5 (cubic *Ia*3*d* gyroid-surface morphology), and HOM-10 (cubic *Fm*3*m*, SBA-12- and FDU-2-like hexagonal intergrowth and pure phase structure). Such successful fabrication is evidence of the effective use of instantly direct templates of the liquid crystal phase for the synthesis of various mesoscopically ordered silica. In addition, the HOM structures fabricated here revealed retention of long-range ordering after high-temperature treatments and long-term exposure to severe hydrothermal conditions such as boiling water and steam.

Experimental Section

1. Chemicals. All materials were used as produced without further purification. Triblock copolymer ($EO_mPO_nEO_m$) surfactants and tetramethyl orthosilicate (TMOS), which was used as the silica source, were obtained from Sigma-Aldrich Company Ltd. USA. The surfactants were Pluronic P123 ($EO_{20}PO_{70}EO_{20}$, M_{av} = 5800), Pluronic F68 ($EO_{80}PO_{27}EO_{80}$, M_{av} = 8400), and Pluronic F108 ($EO_{141}PO_{44}EO_{141}$, M_{av} = 14.600), where EO is $-CH_2-CH_2O-$ (hydrophilic part, or corona), and PO is $-CH_2-CH_2-CHO-$ (hydrophobic part, or core). However, the EO content was 30, 80, and 83 wt % for P123, F68, and F108 copolymers, respectively.

2. Monolithic Silica Synthesis. In general, translucent silica/copolymer monolithic mesophases were fabricated by direct templating of the *instantly preformed liquid crystal phase* method previously reported.[24] In brief, this fabrication procedure involved adding TMOS to triblock copolymers to obtain a well-homogenized sol−gel mixture, particularly with mixture domains formed from a highly specific copolymer/TMOS mass ratio between 35 and 90 wt % (Table 1). Rational solubilization (homogeneity) was obtained, particularly with high surfactant concentration (90 wt %) with continuous stirring and agitation at 50−60 °C, by using a water bath for approximately ~1 min. An acidified aqueous solution (adjusted to pH 1.3 by HCl at 37.6%) was added to the mixture domains to quickly achieve the desired liquid crystal phase and then to promote hydrolysis of the TMOS around the liquid crystal phase assembly of the triblock copolymer surfactants. The molar ratio TMOS:H_2O was held constant at 2:1 in both lyotropic phase synthesis systems.

Typical conditions used for the synthesis of transparent monoliths from one phase formed at a specific copolymers/TMOS mass ratio of 80 wt % in lyotropic systems were as follows. First, 1.6 g of copolymer and 2 g of TMOS were dissolved in a flask by agitation in a water bath (50−60 °C) for 1 to 2 min, yielding a clear solution (i.e., homogeneous). To this mixed solution was quickly added 1 g of H_2O/HCl. The

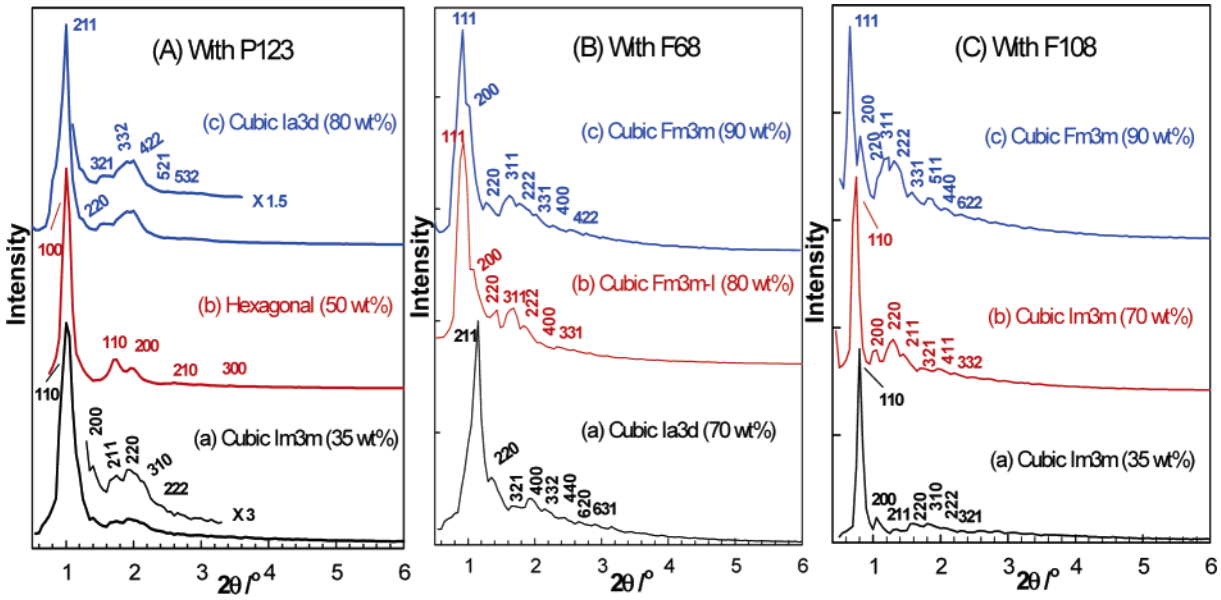

Figure 1. XRD patterns of calcined silica cage and cylindrical monoliths synthesized by using lyotropic mesophases of copolymers of (A) P123 template at P123/TMOS ratios of 35, 50, and 90 wt % for fabrication of cubic *Im*3*m* (a), 2D hexagonal *P*6*mm* (b), and cubic *Ia*3*d* (c), respectively, of (B) F68 template at F68/TMOS ratios of 70, 80, and 90 wt % for fabrication of cubic *Ia*3*d* (a), cubic *Fm*3*m*−*I* with intergrowth (b), and cubic *Fm*3*m* (c), respectively, and of (C) F108 template at F108/TMOS ratios of 35, 70, and 90 wt % for fabrication of cubic *Im*3*m* (a, b) and cubic *Fm*3*m* (c), respectively.

mass ratio of surfactant:TMOS:H_2O/HCl was 1.6:2:1. Synthesis of all HOM monolithic samples at various surfactant/TMOS ratios was done with the same procedure similar to that mentioned in such exemplary composition given with 80 wt %. The amount of the block copolymers was varied at 0.7, 1.0, 1.4, and 1.8 in the mixture composition to fabricate mesophases with copolymer/TMOS mass ratios of 35, 50, 70, and 90 wt %, respectively, as listed in Table 1. Without the static condition (i.e., no aging time) used for the composition mixture, the methanol produced from the TMOS hydrolysis was removed by using a diaphragm vacuum pump connected to a rotary evaporator at ambient synthesis temperature (Table 1). Within ~10 min, the resulting viscous liquid changed to an optical gellike material (solid product) and acquired the shape and size of the round-balloon flask. To obtain macroscopic, crack-free, and shape-controlled silica translucent monoliths at centimeter dimensions, the gentle drying of the resultant translucent silica/copolymer mesophase monoliths was necessary at room temperature for 3 h and then the product was allowed to stand in a sealed container at 40 °C for 10 h to complete the drying process.[24] The copolymers were removed by calcination at 450 °C (1 h under nitrogen and then 6 h under oxygen).

3. Thermal and Hydrothermal Treatments of Monoliths. Before the hydrothermal treatment, the calcined monolithic samples were ground into a powder. The resultant samples (250 mg) were then refluxed in deionized water at 100 °C under agitation for different periods of time (i.e., from 1 to 32 days). After this refluxing, the samples were filtered and dried at 120 °C before any characteristic analyses were measured. However, for the structural stability under steam, the samples were also exposed to water vapor in N_2 steam at 800 °C for 10 h. The N_2 steam was at a constant flow rate (90 mL/min) and was bubbled in a water bath, which was temperature-controlled at 100 °C to achieve the high concentration of water vapor.

To check the thermal stability, the calcined monolithic samples were heated under N_2 at different higher temperatures such as 600, 800, 900, and 1000 °C for 10 h. The heating rate was 1 deg C min^{-1}.

Analyses. Small-angle powder X-ray diffraction (XRD) patterns were measured by using an MXP 18 diffractometer (Mac Science Co. Ltd.) with monochromated Cu Kα radiation with scattering reflections recorded for 2θ angles between 0.3° and 6.5° corresponding to *d* spacings between 29.4 and 1.35 nm. N_2 adsorption−desorption isotherms were measured with a BELSORP36 analyzer (JP. BEL Co. Ltd) at liquid N_2 temperature (77 K) by using the Barrett−Emmett−Teller (BET) method of surface area and the Barrett−Joyner−Halenda (BJH) analyses of pore size distributions from the adsorption curve of the isotherms. All samples were pretreated at 300 °C for 8 h under vacuum until the pressure was equilibrated to 10^{-3} Torr. Transmission electron microscopy (TEM) images were obtained by using a JEOL TEM (JEM-2000EXII) operated at 200 kV with a side-mounted CCD Camera (Mega View III from Soft Imaging System Co.). The TEM samples were prepared by dispersing the powder particles onto holey carbon film on copper grids. ^{29}Si MAS NMR spectra at room temperature were also measured with a Bruker AMX-500 operated at 125.78 MHz with a 90° pulse length of 4.7 μs. For all samples, the repetition delay was 180 s with a rotor spinning at 4 kHz. The chemical shift scale was externally set to zero for the ^{29}Si signal by using tetramethylsilane.

Results and Discussion

1. Control Over Copolymer/Silica Mesophase Morphology. The instant direct-templating liquid crystalline phase strategy revealed new insight into actual control of mesophase structural morphology and mesopore organization,[24] and such control is an extension of the direct templating method.[25,26] However, when the lyotropic liquid crystalline phases of block copolymers ($EO_mPO_nEO_m$) were used in this study, fabrication of a wide range of different mesostructured ordered monoliths was feasible at various synthesis conditions (Table 1) (evidence from XRD and TEM profiles, Figures 1−3). For all synthesis designs, the XRD patterns of these HOM monoliths (Figure 1) show well-resolved, sharp Bragg peaks that allowed identifica-

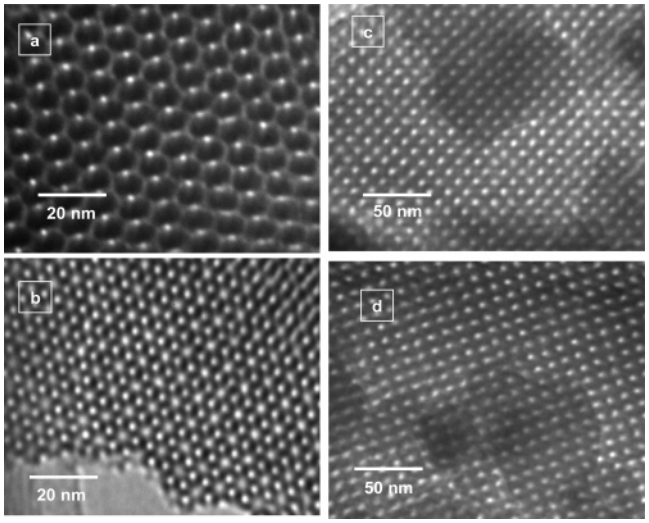

Figure 2. Representative TEM images of silica monoliths viewed along the (a) [110] and (b) [111] directions of a cubic *Ia*3*d* cage (HOM-C5) and cylindrical (HOM-5) monoliths synthesized in lyotropic systems of F68 and P123 copolymers, and viewed along the (c) [100] and (d) [110] projections of cage cubic *Im*3*m* (HOM-C1) monoliths synthesized by using F108 copolymer at F108/TMOS of 35 wt %.

tion of certain HOM structures likely to have analogous and closely reflected planes (as listed in Table 1). These unique reflection planes were characteristic of highly ordered 2D hexagonal and 3D cubic phase domains with a large lattice constant up to 27 nm for calcined monoliths (Table 1). Our results also show that following calcination, the structural contractions for all HOM monolithic lattice dimension constants generally ranged between 10% and 12% depending on the synthesis compositions of the mesophase domains (Table 1), yet the structures retained their well-defined ordering.[20,24] Despite this shrinkage of the HOM frameworks, the intensity and resolution of the reflection peaks become more intense, indicating a high degree of mesoscopic order after removal of the copolymer species (Figure 1).

The XRD profiles here (Figure 1A−C) provided evidence that by varying the phase composition domains, uniform micelle aggregates can be formed from core (PO) and corona (EO) and can then be "tuned" to different mesophase geometries according to the characteristics of the copolymers used as structure-directing agents. Upon change in copolymer concentration in the lyotropic phase domains, both the volume fractions of the sphere core and corona and the packing interassembly interactions depended on systematic changes in the radii of the core/corona blocks and on the number of micelle aggregates.[27] Those systematic changes led to several significant features of the copolymer/silica lyotropic systems: (i) increase in the micellar size and volume fraction causes an increase in interlayer *d* spacing (i.e., swelling) of the mesophase structure of a composition that has higher copolymer concentration, as evidenced by an increase in the lattice constants (Table 1); (ii) the micellar aggregate-assembly at each phase composition domain might act as a driving force for the preferred shape formation based on the molecular geometry of the phase structures; and (iii) the EO-PO blocks could significantly influence the ability to design various ordered mesophase geometries in these copolymer synthesis systems.[27b,c] For example, with P123 copolymer, in which the hydrophobic part (PO blocks) is almost three times larger that the hydrophilic part (EO blocks), the lower curvature-surface phase was formed with increasing P123 concentration in the composition phase domains (i.e. *cubic Im*3*m*−hexagonal *P*6*mm*−cubic *Ia*3*d* phase systems, Figure 1A). However, when the concentration of the P123 template was increased, the number of PO blocks within the micellar core increased, which in turn increased the micellar size, thus leading to high molecular packing and a low curvature-surface phase. In contrast, with the largest EO/PO compositions of F68 and F108 copolymers, the aggregation of high interfacial-curvature-surface phases was evident, especially at the high concentration of copolymers F68 and F108 used (i.e., *Ia*3*d*−*Fm*3*m* and *Im*3*m*−*Fm*3*m* phase transitions, Figure 1, panels B and C, respectively).[27] Based on these topological mesophases formed with the present copolymers, the types of phase structures of surfactant, in general, were significantly influenced by the preferred interfacial curvature according to the surfactant geometry. However, the extra degree of conformational freedom is likely responsible for the unique structural polymorphism formed.[27d] This degree of conformational freedom enabled significant control over the rearrangement and deformation of the micelle form, according to the constraint effects during the synthesis conditions, such as synthesized composition domains, temperature, and solution pH, that affect the phase structure, and then further determine the phase topology of the surfactants. This explains why those specific mesostructured phases can be subsequently formed in the P123, F68, and F108 synthesis systems by using the instant direct-templating strategy.[27]

2. Highly Ordered Silica Monolithic Pore Architectures (HOM). TEM micrographs (Figure 2) reveal well-organized mesopore arrays over a large area of those cubic lattices. TEM images (Figure 2a,b) reveal ordered 3D pore networks with channels running along the [110] and [111] zone axes directions of cubic *Ia*3*d* (HOM-5) monoliths. These representative TEM images oriented with those preferable zone axes provide direct evidence that gyroidal minimal surface (G-surface) can describe the cubic morphology of HOM-5 monoliths with *Ia*3*d* symmetry.[12,28,29] Thus, the TEM images (Figure 2c,d) of cubic *Im*3*m* monoliths (HOM-1) reveal a high degree of symmetry and order oriented along the [100] and [110] lattice planes, agreeing well with previous TEM micrograph images of the SBA-16 structure, which has (bcc) cubic *Im*3*m* symmetry with I-WP minimal surface morphology.[30] The lattice constants derived from the TEM patterns (Figure 2) are similar to those determined from the XRD profiles (Table 1), suggesting the formation of the single phase of cubic *Ia*3*d* and *Im*3*m* structures.

Significantly, TEM micrographs of cubic *Fm*3*m*−*I* (fcc) mesophase (HOM-12) synthesized by using the F68 template at a F68/TMOS ratio of 80 wt % reveal that spherical mesopore channels were interconnected with hexagonal close-packed pore architectures (Figure 3 b), although the XRD pattern (Figure 1Bb) of this material clearly exhibited peaks similar to the highly ordered cubic *Fm*3*m* materials fabricated with F68 and F108 copolymers at 90 wt % (Figure 1B,C). However, large-scale domains of high-intensity spots that can be indexed as a cubic (fcc) lattice of *Fm*3*m* symmetry along the [100] and [111] directions (Figure 3a,c) were clearly observed. In turn, based on the spherical ordered arrays viewed along the [111] direction (Figure 3b), the perfect hexagonal close-packed arrays of channel-like pores oriented along the [001] plane clearly identified with the fcc crystal with *Fm*3*m* point groups. Clearly evident was that the distance between pores oriented around the (hcp) arrays was in a good agreement with the d_{111} of the fcc sample of *Fm*3*m*−*I* mesophases (Figure 1Bb). These observations clearly indicate that the silica monoliths synthesized by using F68 copolymer at F68/TMOS of 80 wt % as templates were dominantly fcc phases growing with the 3D hexagonal

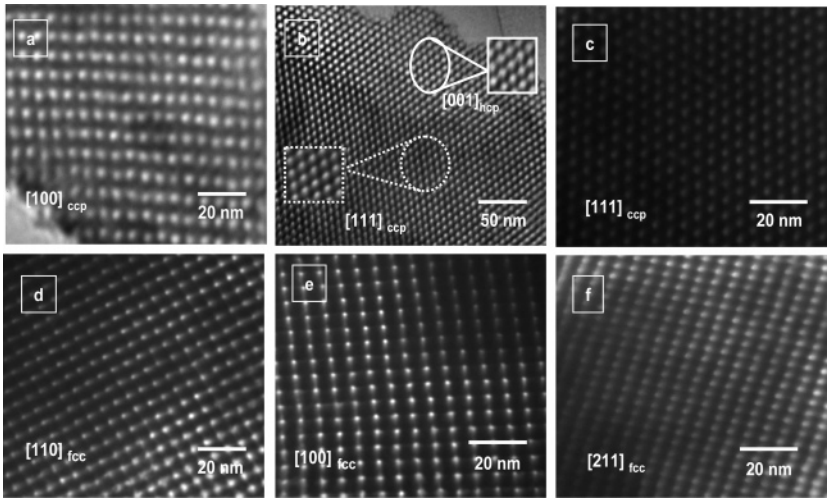

Figure 3. TEM images oriented along the (a) [100] direction associated with cubic close-packing structure (ccp), (b) along the incidence of cubic/hexagonal intergrowth structure of [111]ccp/[001]hcp zone axes, and (c) the [111] direction associated with the ccp structure of cubic *Fm*3*m* symmetry synthesized in the lyotropic system of F68 copolymer at F68/TMOS of 80 wt % (HOM-12). TEM images viewed along the (d) [110], (e) [100], and (f) [211] directions of a single cubic *Fm*3*m* silica mesophase with cage (HOM-C10) and cylindrical (HOM-10) monoliths synthesized by using lyotropic or microemulsion of F108 and F68 at 90 wt %.

architectures as conclusively deduced for cubic *Fm*3*m* (FDU-1) materials.[8b] Figure 3d−f (corresponding to the [110], [100], and [211] planes, respectively) gives the most informative images for the fcc structures fabricated with F108 and F68 systems at a higher concentration of 90 wt %. These two images reveal the uniform spherical pore architectures that are characteristic of large single-domain cubic fcc mesophases.[13,24,31] The structural pores was dominated by a spherical arrangement with remarkable crystal orientations (i.e. no defect), and had no hexagonal pore channels, indicating a highly ordered cubic structure (fcc) of *Fm*3*m* space group without hexagonal intergrowth features (HOM-10).

In the interior of the topological growth phases (HOM-12) formed with the F68 lyotropic system, an increase in F68 concentration induced an abrupt change in the interfacial surfaces from cubic *Ia*3*d* to *Fm*3*m* symmetry (Figure 1Ba−c). This change might gradually permit further annealing of mesostructures likely to be a 3D hexagonal phase domain with the cubic *Fm*3*m* structure (Figure 1Bb), designated as the cubic *Fm*3*m*−*I* mesophase. This cubic *Fm*3*m*−*I* phase structure underwent the transition to the single phase cubic *Fm*3*m* structure by an increase of the F68 concentration to 90 wt % (as listed in Table 1) and by addition of alkanes in microemulsion systems (which observed the same TEM images as shown in Figure 3d−f). With such phase transitions, the d_{111} spacing values of fcc structures were unremarkably changed (Figure 1Bb,c), despite the effect of the higher F68 copolymer concentrations used. In turn, results from our syntheses with F108 template suggest that at high F108 concentration (Table 1), the change in the mesophase geometry occurring between relatively similar curvature surfaces of phases (i.e., *Im*3*m*−*Fm*3*m* system) might probably facilitate the formation of a wide range of stability of single cubic *Fm*3*m* phase domains in lyotropic (cosolvent-free) systems.

3. Shape- and Size-Controlled Cage and Cylindrical Pore Geometries. On the basis of the N_2 isothermal results, the HOM monolithic structures well-fabricated by using the *instant direct-templating method* exhibited appreciable textural parameters of specific surface area (S_{BET}), mesopore/micropore volumes, and thick walls (Table 1). The microporosity of HOM monoliths was assessed (using the *a*s-plot method) to be in the 0.04−0.16 cm^3/g range.[32] The increase of the micropore voulmes was strongly affected by the unit numbers of EO_m blocks of the copolymer templates used, ruling out the potential effect of the penetration of the hydrophilic (EO) blocks into the silica wall during fabrication of the silica/copolymer mesophases (Table 1). In general, typical type IV adsorption behavior and a pronounced hysteresis loop with a well-known sharp inflection of adsorption/desorption branches were features of the isotherms of HOM samples and are characteristic of the uniformity and regularity of materials. The adsorption branches were significantly shifted toward higher relative pressure (P/P_o) with a high concentration of copolymers used in the composition phase domains, and with the large size of the PO−EO blocks (core-corona) of the copolymer templates.

Wide type H_2 hysteresis loops and the well-defined steepness of isotherms (Figure 4) indicate large and uniform cage structures similar to those for prominent FDU-1 silicas.[8b,32] The width of the hysteresis loop increased with increasing mesopore size for all monolithic structures templated by the F68, F108 copolymers. The distinctive similarity in the isothermal shape and in P/P_o (0.45−0.5 range) of the capillary evaporation of HOM-C structures fabricated at various synthesis conditions validated that the sizes of the entrances of the pores that connect the uniform caged pores were below 4.0 nm, despite the increase in the size of spherical cavities of the pore cages up to 10 nm (Table 1). These isothermal shapes provide strong evidence that the stability of the cage-like pore domains was dependent on the molecular nature of templated copolymers. A wide range of cage mesophase domains can be substantially fabricated with the highest EO/PO block compositions of F108 copolymer (Figure 4C); however, cubic *Im*3*m* (HOM-C1) and *Ia*3*d* (HOM-C5) cage monoliths were fabricated at only 35 wt % and up to 70 wt % of composition phase domains of P123 and F68 copolymer templates (Figure 4A,B), respectively. The 3D cage-like pore frameworks were likely to have more open-pores with cubic *Ia*3*d*, *Im*3*m*, and *Fm*3*m* structures fabricated by using a high concentration of F68 and F108 copolymers (Figures 4Bb,- and 4Cc−e). However, the shift toward higher P/P_o for the desorption isotherms was due to the pore blocking effects,[32] indicating that other enlarged pore entrances (bimodal or trimodal) with sizes up to 9.8 nm were connected with the spherical cavity of the cage structures.[8b] Such isotherm behavior has been clearly observed for the cage-like framework silica

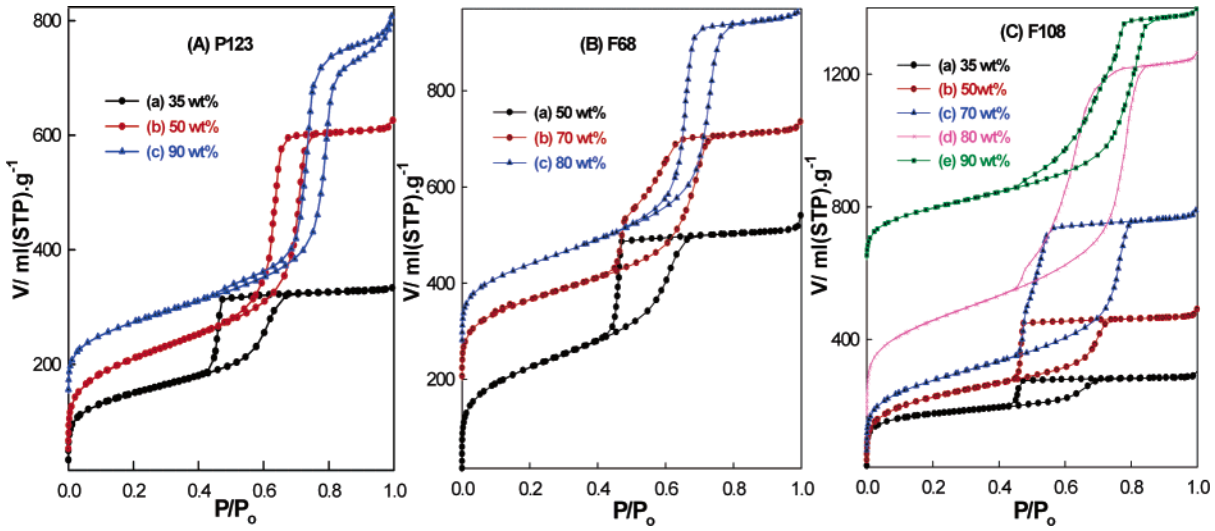

Figure 4. N_2 adsorption/desorption isotherms of cage-like (HOM-C) and cylindrical-like (HOM-n) pore monoliths synthesized by using lyotropic mesophases of copolymers of (A) P123 template at P123/TMOS ratios of 35, 50, and 90 wt % for fabrication of cage cubic *Im*3*m* HOM-C1 (a), cylindrical 2D hexagonal *P*6*mm* HOM-2 (b), and cylindrical cubic *Ia*3*d* HOM-5 (c) materials, respectively, of (B) F68 template at F68/TMOS ratios of 50 and 70 wt % for fabrication of cage cubic *Ia*3*d* HOM-5 (a, b) and of 80 wt % for fabrication of cylindrical cubic *Fm*3*m*−*I* with intergrowth HOM-12 (c) materials, respectively, and of (C) F108 template at F108/TMOS ratios of 35−80 wt % for fabrication of cage cubic *Im*3*m* HOM-C1 (a−d) and of 90 wt % for fabrication of cage cubic *Fm*3*m* HOM-C10 (e) materials, respectively. Isotherms (A) for (b) and (c) were shifted vertically by 10, 120 mL STP g^{-1}, respectively. Isotherms (B) for (b) and (c) were shifted vertically by 170 and 250 mL STP g^{-1}, respectively. Isotherms (C) for (c), (d), and (e) were shifted vertically by 30, 160, and 600 mL STP g^{-1}, respectively.

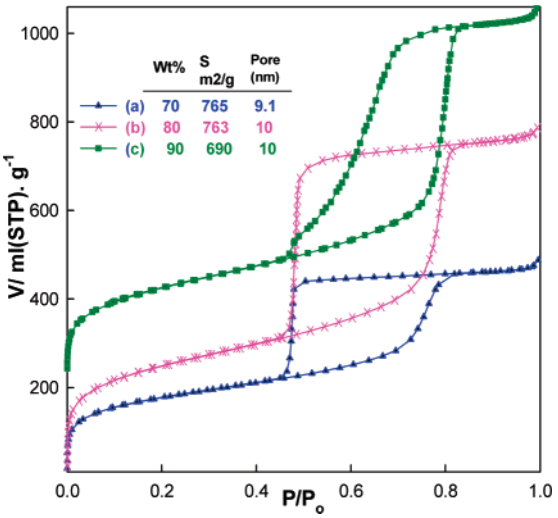

Figure 5. N_2 adsorption/desorption isotherms of cage-like (HOM-C) pore monoliths synthesized in microemulsion systems formed by addition of C_{12}-alkane (dodecane) to the lyotropic phases of F108 copolymer at F108/TMOS of 70 (a), 80 (b), and 90 wt % (c), respectively. Isotherm (d) was shifted vertically by 200 mL STP g^{-1}, respectively.

FDU-1 and PSU-1 structures fabricated at various hydrothermal-treatment temperatures.[8b,21,22] Interestingly, in the microemulsion systems formed by addition of C_{12}-alkane (dodecane) to the more open-pore cage domains of F108 template (Figure 4Cc−e),[33] significant changes in the connecting pore systems (bimodal or trimodal) were revealed for those 3D cubic mesopore cages according to the lower P/P_o for the capillary evaporation of isotherms (Figure 5). However, the hydrocarbon was likely to be evenly distributed within the copolymer mesophase aggregates, thus enabling conformation changes in the cage nature, while no increase in the size of the spherical interior pores was observed according to this solubilization action of hydrocarbons (see Figure 5 insert, and Table 1). This result rules out the potential control over the connecting-pore sizes of the cage monoliths under the instant direct-templating design strategy.

Figure 4A,B shows evidence that the HOM-C cage structures completely underwent transformation to ideal open cylindrical channel-like pores (HOM-n) over a wide range of phase domains formed with relative increase of the P123 and F68 copolymer concentrations, as evidenced from the isothermal shapes with well-defined type H_1 hysteresis loops.[34] In addition, the isotherms with a well-characterized sharp inflection point appearing at $0.6 \leq P/P_o \leq 0.8$ (Figures 4Ab,c, and 4Bc) strongly indicate that uniformity of the cylindrical structures with 2D and 3D geometries could be attained with the increase in the open pores. In general, the enlargement of the cylindrical and cage pore sizes by using a higher concentration of copolymers indicates that an increase in micelle aggregation of triblock copolymers causes a significant increase in pore size in the absence of swelling agents. For given copolymer templates, the pore sizes increased as a function of the core (PO) and corona (EO) block lengths, whereas the pore size was effectively influenced by the hydrophobic block (PO) length. The effect of EO-block on the pore sizes of HOM monoliths contrasts with materials synthesized by using $EO_mBO_nEO_m$ copolymers,[35] where the pore size of that material decreases with large EO-blocks of template, but was consistent with the nanocasting silica mesophases fabricated by using alkyl-oligo(ethylene oxide) (C_x-EO_y) surfactants as templates.[36]

4. Thermal and Hydrothermal Stability of HOM Monoliths. The long-range highly ordered HOM monoliths exhibited significant retention in their structural periodicity and long-term stability in their local mesopore framework architectures without degradation, despite the lack of atomically ordered organization in the framework walls of those materials. However, the retention of a high degree of mesoscopic order was observed for HOM materials even after calcination at a high temperature of 1000 °C. XRD patterns (Figure 6A) clearly revealed that high-temperature treatments caused the cage cubic *Im*3*m* (HOM-C1) diffraction planes to shift to higher 2θ values, as evidenced by the reduction in the d_{110} spacing and in the lattice constants (Table 2). This result indicates that the heat treatment at higher temperatures led to further densification of silica frameworks

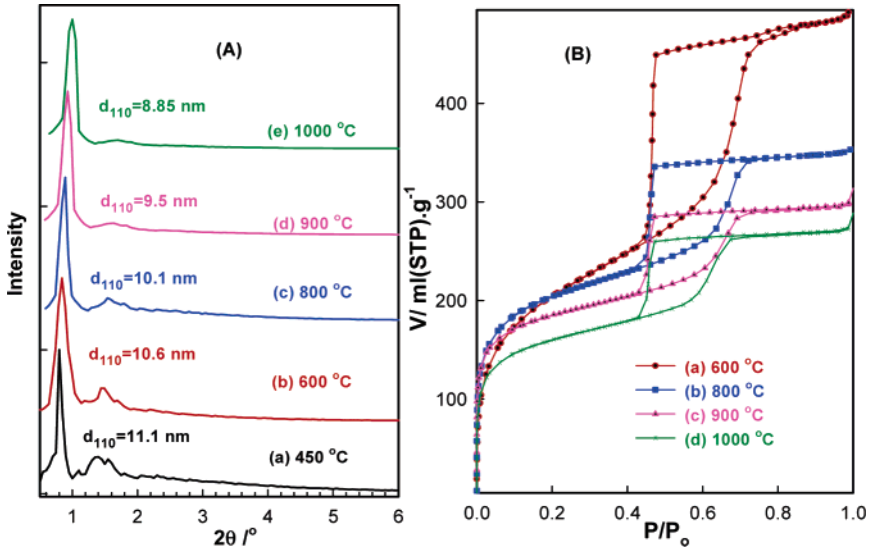

Figure 6. (A) XRD patterns and (B) N_2 adsorption/desorption isotherms of calcined mesoporous silica monoliths with cubic *Im*3*m* cage structures (HOM-C1) fabricated in the lyotropic system of F108 copolymer at F108/TMOS of 50 wt %, after calcination at high-temperature treatments from 450 to 1000 °C.

TABLE 2: Effect of Thermal and Hydrothermal Treatments (steam in N_2, and boiling H_2O) on the Structural Properties of Cage Cubic *Im*3*m* (HOM-C1) Silica Monoliths Synthesized in Lyotropic Mesophases of F108 at F108/TMOS Ratios of 50 and 80 wt %[a]

treatment conditions	α_o, Å	S_{BET}, m^2/g	V_P, cm^3/g	V_m, cm^3/g	R, Å	W, Å
calcined HOM-C1[b]						
450 °C	157	784	0.77	0.16	68	89
600 °C	150	750	0.72	0.12	64	86
800 °C	143	645	0.50	0.10	60	83
900 °C	134	600	0.40	0.07	58	76
1000 °C	124	550	0.38	0.05	52	72
steamed HOM-C1[b] at 800 °C, 10 h	143	610	0.45	0.05	60	83
boiling HOM-C1[c]						
none	178	996	1.9	0.12	100	78
1 day	175	800	1.7	0.10	110	65
2 days	172	650	1.6	0.08	130	42
4 days	170	550	1.6	0.05	138	32
10 days	168	497	1.8	0.02	138	30
20 days	163	480	1.9		138	25
32 days	156	408	1.9		138	18

[a] All notations are the same as in Table 1. [b] 50 wt %. [c] 80 wt %.

by the condensation of silanol groups. Although the high-temperature calcination significantly increased the degree of framework cross-linkage, the high extent of polymerization of silica walls degraded the framework mesoporosity, consistent with the decrease of the intensity and resolution of the higher order diffraction peaks (Figure 6Ad,e).[37] The N_2 isotherms (Figure 6B) show that increasing the high-temperature treatments had no significant changes in the cage character of cubic *Im*3*m* mesopores; however, the sample underwent the lowering of the adsorption capacity.[38] The gradual shift of the capillary condensation toward lower relative pressure P/P_o by increasing the calcination temperature indicates the decrease of the mesopore spherical cavity sizes (Table 2). However, the capillary evaporation was well-pronounced at lower P/P_o, namely, from 0.45 to 0.5, indicating that narrower connecting pore sizes (below 4 nm) remained substantially unchanged (Figure 6B). In addition, the sharpness in the inflection adsorption steps indicates capillary condensation within uniformly sized mesopores.[38] The slight decrease of the specific surface area, micropore and mesopore volumes, and thinner pore walls indicates a partial collapse of these materials after high-temperature calcination (Table 2). Our results here provide strong evidence that the HOM monolith structures had a higher thermal stability, similar to the stability reported for FDU-1 materials.[38]

Hydrotreated cage cubic *Im*3*m* (HOM-C1) monoliths in high-temperature flowing steam exhibit the high retention of structural ordering despite the severe steam treatment at a high temperature of 800 °C for long-contact time (10 h) of H_2O vapor with siloxane linkages (≡Si−O−Si≡) on the framework surfaces. The TEM images of the hydrotreated HOM-C1 (Figure 7) show high-order large-scale pore domains along the [111] and [100] orientations with little defects in the pore organization (see arrows in Figure 7a,b), indicating the excellent ordering of the cage cubic *Im*3*m* monoliths. This considerable retention of the cage mesopores after hydrothermal steaming was similar to the stability of gyroidal cubic *Ia*3*d* monoliths (HOM-5) synthesized by using the microemulsion phase of the P123 template.[39] The XRD patterns for the HOM-C1 monoliths treated with steam showed no significant changes in the resolution of the diffraction peaks and d_{110} value (101 Å) compared with those of high-temperature calcination monoliths at 800 °C (as shown in Figure 6Ac). Moreover, the N_2 isotherms of these hydrotreated HOM-C1 monoliths provide further evidence of the retention of the structural mesoporosity of the cubic *Im*3*m* frameworks after

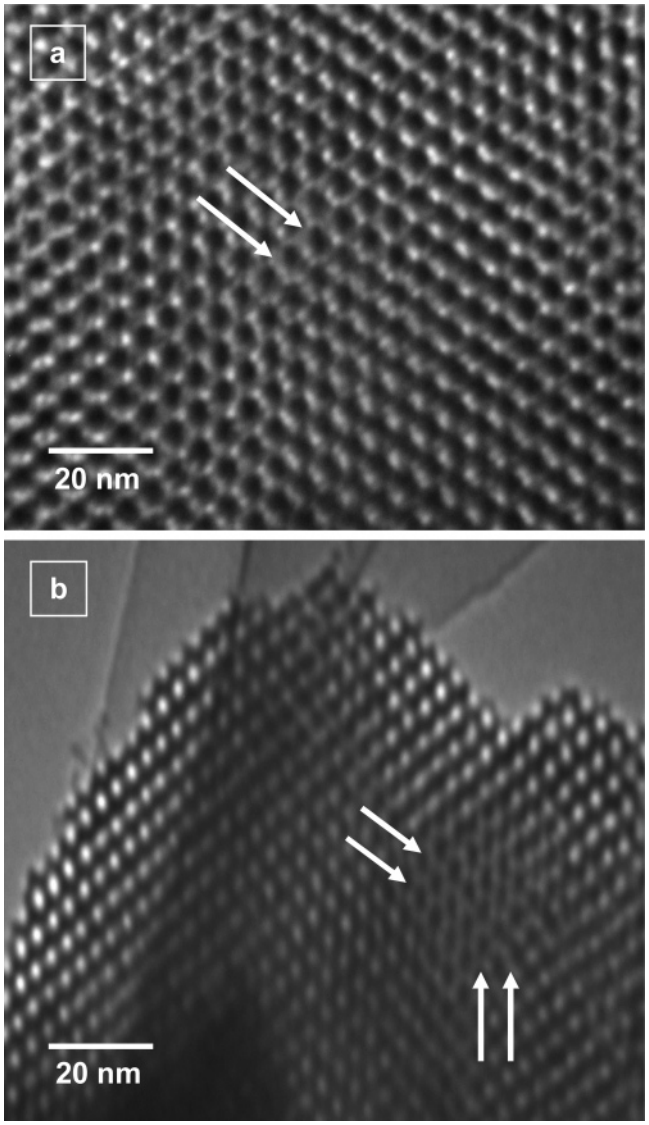

Figure 7. TEM images recorded along the (a) [111] and (b) [100] zone axes of cage cubic *Im*3*m* monoliths (HOM-C1) synthesized in the lyotropic system of F108 copolymer at F108/TMOS of 50 wt % after hydrothermal treatment in flowing steam (under water vapor in N_2 flow at 800 °C for 10 h). Arrows indicate the slight distortion in orientational grains along the incidences caused by the hydrothermal steam.

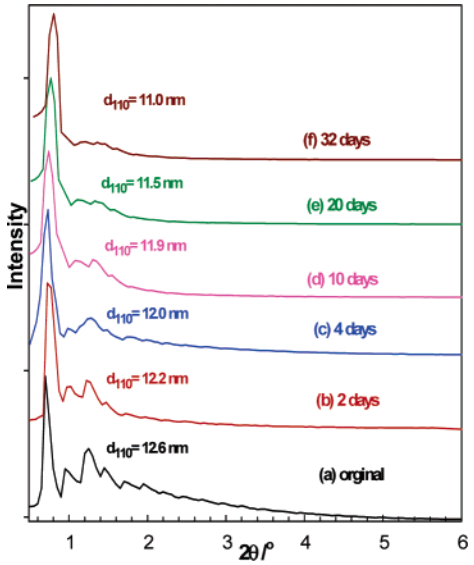

Figure 8. XRD patterns of calcined cubic *Im*3*m* cage structures (HOM-C1) synthesized in the lyotropic system of F108 copolymer at F108/TMOS of 80 wt % (a) and after hydrothermal treatment in boiling water from 2 to 32 days.

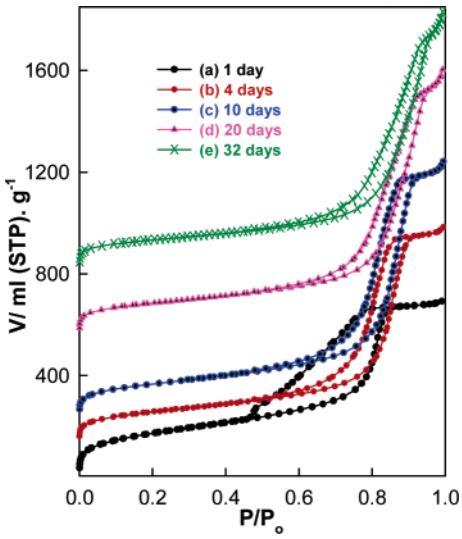

Figure 9. N_2 adsorption/desorption isotherms of calcined cubic *Im*3*m* cage structures (HOM-C1) synthesized in the lyotropic system of F108 copolymer at F108/TMOS of 80 wt % after hydrothermal treatment in boiling water from 1 to 32 days. Isotherms (b), (c), (d), and (e) were shifted vertically by 130, 230, 570, and 830 mL STP g^{-1}, respectively.

hydrothermal steaming treatments. Both the pore volume and the surface area slightly decreased (Table 2), yet the pore sizes remained virtually unchanged, indicating that a high-temperature flowing steam (under water vapor in N_2 flow at 800 °C) has much more effect on the pore volume and surface area than on the pore sizes. The shape and breadth of the hysteresis loops of HOM-C1 samples treated at 800 °C (Figure 6Bb) and the hydrothermal steaming samples were identical, indicating the significant retention of the cage mesostructure frameworks.

On the contrary, our results show that a drastic degradation in textural properties of HOM pore frameworks was observed under hydrothermal treatment in boiling water for a long time; however, this degradation did not ultimately lead to loss or collapse of the mesostructured geometry (Figures 8−10). To evaluate the hydrothermal stability, we investigated cubic *Im*3*m* HOM-C1 monoliths (synthesized at F108/TMOS of 80 wt %) that had a large cage with more open-pore entrances under hydrothermal conditions for 1 to 32 days in boiling water. The XRD patterns (Figure 8) show that the cubic *Im*3*m* samples treated in boiling water for 1 to 10 days attained significant planes that suggest long-range ordering, despite indistinct low intensity peaks in the $1.5 \leq 2\theta \leq 3$ range. Upon long treatment time (>10 days), the intensity and resolution of the diffraction peaks were less pronounced, yet remarkable peaks indicating the fidelity of the cubic *Im*3*m* geometry were retained. The decrease in d_{110} value and lattice constants (Table 2) were due to the degradation in the internal pore-wall architecture.

The N_2 isotherms of these hydrotreated monoliths in boiling water (Figure 9) reveal significant changes in the hysteresis loop from H_2- to H_1-type with a well-developed step at $0.75 \leq P/P_o \leq 0.85$ that is characteristic of capillary condensation into uniform mesopores. Both sets of isotherms indicate the transition of the large-pore cages (cavity ~10 nm) characteristic of more open-pore sizes with entrances larger than ~5 nm to open-cylindrical mesopores after boiling for 1 day, while the resulting cubic *Im*3*m* geometry virtually did not change, as evidenced

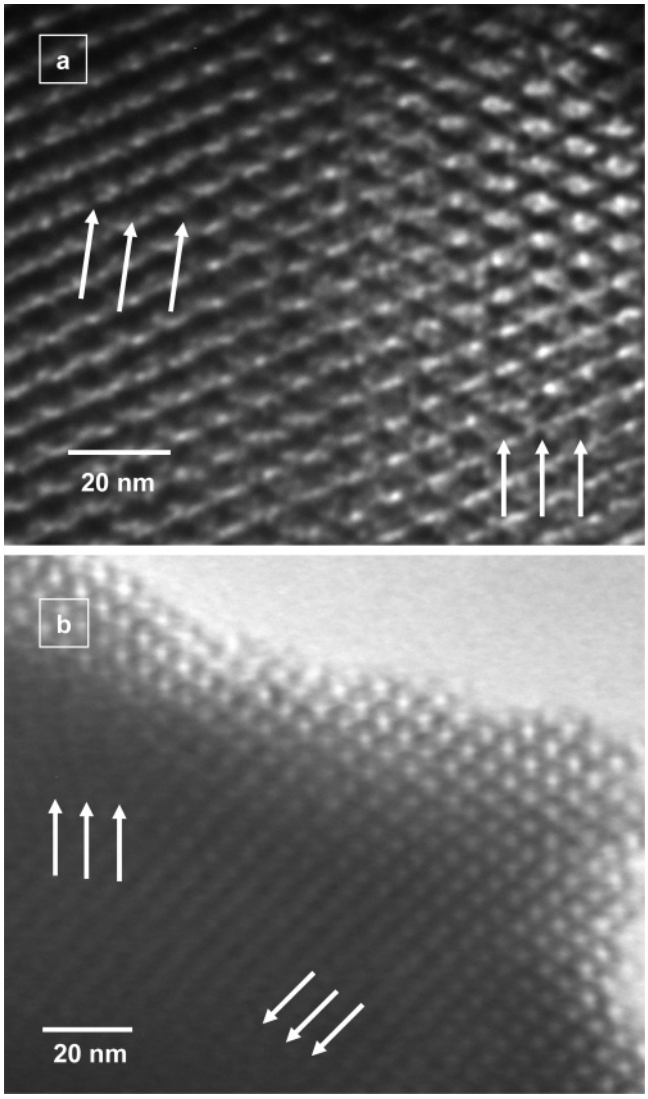

Figure 10. TEM images recorded along the (a) [111] and (b) [100] zone axes of cage cubic *Im*3*m* monoliths (HOM-C1) synthesized in the lyotropic system of F108 copolymer at F108/TMOS of 80 wt % after hydrothermal treatment in boiling water for 1 day. Arrows indicate the significant distortion in orientational grains along the incidences caused by the hydrothermal treatment in boiling water for a relatively short period.

from the XRD profiles (Figure 8). This change in the isotherms clearly indicates that the cage geometrical shapes and sizes play a significant role in the retention degree of the character of the cage-like mesoporosity under hydrothermal treatment in boiling water.[22,38] For monoliths treated more than 10 days, the hysteresis loops were narrow, especially the upper parts of $0.85 \leq P/P_o \leq 0.9$, indicating the degree of distortion of the uniformity of the mesostructures, consistent with the XRD peaks (Figure 8e,f), and indicating the broadening of the pore-size distribution curves (data not shown). The textural parameters (Table 2) show that the samples underwent extensive degradation during the boiling water treatment. Thereby, the structure frameworks, which could possibly collapse, exhibited large pore volumes, relatively small surface area, and pore-thinning walls, as expected for those large pore sizes of monoliths hydrotreated with boiling water compared to the primary cubic *Im*3*m* structures (Table 2). The microporosity was drastically decreased, suggesting that degradation influences the pore wall of materials. The high extent of degradation was also evidenced by TEM micrographs of these hydrotreated monoliths (Figure 10). The images reveal a significant distortion affected the orientational pore ordering by boiling even for relatively lower times (24 h) compared to the steam treatment sample (Figure 7). However, the TEM images also observed ordered pore channels over sufficiently large domains, indicating that the mesopore uniformity was retained for these mesostructure frameworks.

Clearly evident from our results was that the hydrothermal treatment under boiling water has a much greater effect on the textural properties of HOM materials than steaming (Table 2). This suggests that the HOM monoliths are relatively stable in high-temperature steam compared with treatment in boiling water. In fact, the dissolution (hydrolysis) of HOM silica pore frameworks could have easily occurred during the direct contact of boiling water, particularly for long-term exposure (more than 24 h); however, further increase in the contact-time treatment in boiling water caused the hydrolysis of the siloxane (≡Si−O−Si≡) bridges and subsequent formation of the terminal silanol groups (Si−OH). At the boiling temperature of water, dehydroxylation of Si−OH on surfaces is not likely to occur, thus leading to degradation in the silica framework under further hydrothermal treatments.[40,41] In turn, the high-temperature steaming (at 800 °C) helps further restoration of the siloxane linkages on the silica surfaces by the dehydroxylation process, which restrains the extent of the dissolution.

In general, our results reveal direct, real-space evidence that the HOM materials had thicker pore walls and a high degree of cross-linking frameworks, and thus indeed improved the practical quality of the structural stability.[40] However, in the instant direct-templating synthesis designs, the silica condensation conditions were adequate to improve the interactions between silica and copolymer species, and to fabricate highly ordered silica monoliths (HOM) with thick-walled network matrices, while no aging times or hydrothermal synthesis were used (see Experimental Section). ^{29}Si NMR spectra show evidence of the polymerization silica species forming rigid condensed framework matrices under our synthesis designs. The spectra show that a main resonance at −110 ppm for a Q_4 [Si $(OSi)_4$] environment of the silica framework and a shoulder at −101 ppm for a Q_3 [$(OH)Si\ (OSi)_3$] environment from surface hydroxy groups were revealed after removal the organic moiety, indicating higher Q_4/Q_3 values of ∼6. This suggests that the HOM samples had fully cross-linked framework walls, and is consequently indicative of much more rigid siloxane linkages that would be necessary to stabilize the architecture wall to withstand severe thermal and hydrothermal treatment without loss of structural mesoporosity.

Conclusion

The fabrication of silica monoliths that adopt the *instant preformed liquid crystal phase* in lyotropic systems as templates has been extended by using triblock copolymers ($EO_mPO_nEO_m$) with various molecular natures in structure-directed assemblies. This instant direct-templating method provides realistic control over a wide range of mesophase geometries, yet maintains the long-range structural ordering, and thus improved the simplicity, significant periodicity, and high uniformity of mesoporous silica monoliths. Overall, structures feasibly achieved in those copolymer systems were optically translucent monoliths (crack-free at the macroscopic scale) in 2D hexagonal *p*6mm and 3D cubic mesophases including the body-centered cubic *Im*3*m* structure, cubic bicontinuous G-surface of *Ia*3*d* symmetry, and face-centered cubic *Fm*3*m* structure formed with/without intergrowth of the 3D hexagonal phases. These monoliths exhibited

good quality mesostructure properties, including large mesopore and micropore volumes up to 2.0 and 0.16 cm^3/g, respectively, high surface area, uniform mesopores even with enlarged pores, and thick-wall architectures. Several key factors in these synthesis systems apparently determine the type of phase structure and parameters; the copolymer concentrations in the phase domains and the copolymer molecular nature, such as the EO/PO ratio, significantly affect the formation of microstructure liquid crystalline phases and their extended long-range ordering in the silica monolith mesophases. The extensive findings here provide strong evidence for the formation of large pore cages (cavity up to 10 nm in diameter) with narrow entrances of unimodal (<4 nm), bimodal, or trimodal connecting-pore sizes. The HOM cage structures completely underwent transformation to ideal open cylindrical channel-like pores over a wide range of phase domains formed with a high concentration of lower EO/PO block copolymers. Another finding was that the HOM silica monoliths exhibited considerable retention of both the structural stability and long-range order against higher thermal temperature (up to 1000 °C) and longer hydrothermal treatment times under boiling water and steam. These high-grade mesoscopic monoliths are soon expected to show broad-ranging applications in the development of new material science.

Acknowledgment. We thank our colleagues, in particular, Dr. Y. Kiyozumi, Dr. T. Ikeda, and Dr. T. Nagase (AIST Institute, Tohoku Centre, Sendai), for critical assistance.

References and Notes

(1) (a) Davis, M. E. *Nature* **2002**, *417*, 813. (b) Yamada, T.; Zhou, H. S.; Uchida, H.; Tomita M.; Ueno, Y.; Ichino, T.; Honma, I.; Asai, K.; Katsube, T. *Adv. Mater.* **2002**, *14*, 812. (c) Corna, A. *Chem. Rev.* **1997**, *97*, 2373. (d) Munoz, B.; Ramila, A.; Perez-Partiente, J.; Diaz, I.; Vallet-Regi, M. *Chem. Mater.* **2003**, *15*, 500. (e) Stein, A. *Adv. Mater.* **2003**, *15*, 763.

(2) (a) Kresge, C. T.; Leonowicz, M. E.; Roth, W. J.; Vartuli, J. C.; Beck, J. S. *Nature* **1992**, *359*, 710. (b) Beck, J. S.; Vartuli, J. C.; Roth, W. J.; Leonowicz, M. E.; Kresge, C. T.; Schmitt, K. D.; Chu, C. T. W.; Olsan, D. H.; Higgins, E. W.; Schlenker, J. L. *J. Am. Chem. Soc.* **1992**, *114*, 10834.

(3) Inagaki, S.; Fukushima, Y.; Kuroda, K. *J. Chem. Soc., Chem. Commun.* **1993**, 680.

(4) Huo, Q.; Margolese, D. I.; Feng, P. Y.; Gier, T. E.; Stucky, G. D.; Leon, R.; Petroff, P. M.; Ciesla, U.; Schüth, F. *Nature* **1994**, *368*, 317.

(5) Tanev, P. T.; Pinnavaia, T. J. *Science* **1995**, *267*, 865. (b) Bagshaw, S. A.; Prouzet, E.; Pinnavaia, T. J. *Science* **1995**, *269*, 1242.

(6) Ryoo, R.; Kim, J. M.; Ko, C. H.; Shin, C. H. *J. Phys. Chem. B* **1996**, *100*, 718.

(7) Zhao, D.; Huo, Q.; Jianglin, F.; Chmelka, B. F.; Stucky, G. D. *J. Am. Chem. Soc.* **1998**, *120*, 6024.

(8) (a) Tian, B.; Liu, X.; Yu, C.; Gao, F.; Luo, Q.; Xie, S.; Tu, B.; Zhao, D. *Chem. Commun.* **2002**, 1186. (b) Matos, J. R.; Kruk, M.; Jaroniec, M.; Zhao, L.; Kamiyama, T.; Terasaki, O.; Pinnavaia, T. J.; Liu, Y. *J. Am. Chem. Soc.* **2003**, *125*, 821.

(9) (a) Huo, Q.; Leon, R.; Petroff, P. M.; Stucky, G. D. *Science* **1995**, *268*, 1324. (b) Zhou, W.; Hunter, H. M. A.; Wright, P. A.; Ge, Q.; Thomas, J. M. *J. Phys. Chem. B* **1998**, *102*, 6933.

(10) Soler-Illia, G. J. D. A.; Sanchez, C.; Lebeau, B.; Patarin, J. *Chem. Rev.* **2002**, *102*, 4093.

(11) (a) Zhao, D.; Jianglin, F.; Huo, Q.; Melosh, N.; Fredrickson, G. H.; Chmelka, B. F.; Stucky, G. D. *Science* **1998**, *279*, 548. (b) Zhao, D.; Yang, P.; Melosh, N.; Feng, J.; Chmelka, B. F.; Stucky, G. D. *Adv. Mater.* **1998**, *10*, 1380.

(12) (a) Flodström, K.; Alfredsson, V.; Fällrot, N. *J. Am. Chem. Soc.* **2003**, *125*, 4402. (b) Kleitz, F.; Choi, S. H.; Ryoo, R. *Chem. Commun.* **2003**, 2136.

(13) (a) Kleitz, F.; Liu, D.; Anilkumar, G. M.; Park, I.; Solovyov, L. A.; Shmakov, A. N.; Ryoo, R. *J. Phys. Chem. B* **2003**, *107*, 14296. (b) Fan, J.; Yu, C.; Lei, J.; Tian, B.; Wang, L.; Luo, Q.; Tu, B.; Zhou, W.; Zhao, D. *Angew. Chem., Int. Ed.* **2003**, *42*, 3146.

(14) Yu, C.; Tian, B.; Fan, J.; Stucky, G. D.; Zhao, D. *J. Am. Chem. Soc.* **2002**, *124*, 4556.

(15) (a) Yang, P.; Zhao, D.; Margolese, D. I.; Chmelka, B. F.; Stucky, G. D. *Nature* **1998**, *396*, 152. (b) Li, D.; Zhou, H.; Honma, I. *Nature Mater.* **2004**, *3*, 65.

(16) (a) Nguyen, T. Q.; Wu, J. J.; Doan, V.; Schwartz, B. J.; Tolbert S. H. *Science* **2000**, *288*, 652. (b) Regan, B. C.; Aloni, S.; Ritchie, R. O.; Dahmen, U.; Zettl, A. *Nature* **2004**, *428*, 924.

(17) (a) Coleman, N. R. B.; Morris, M. A.; Spalding, T. R.; Steytler, D. C.; Holmes, J. D. *J. Am. Chem. Soc.* **2001**, *123*, 187. (b) El-Safty, S. A. *J. Colloid Interface Sci.* **2003**, *260*, 184.

(18) (a) Corma, A.; Kan, Q.; Navarro, M. T.; Perez-Pariente, J.; Rey, F. *Chem. Mater.* **1997**, *9*, 2123. (b) Sayari, A.; Yang, Y.; Kruk, M.; Jaroniec, M. *J. Phys. Chem. B* **1999**, *103*, 3651. (c) Blin, J. L.; Otjacques, C.; Harrier, G.; Su, B. L. *Langmuir* **2000**, *16*, 4229.

(19) (a) Schmidt-Winkel, P.; Lukens, W. W., Jr.; Zhao, D.; Yang, P.; Chmelka, B. F.; Stucky, G. D. *J. Am. Chem. Soc.* **1999**, *121*, 254. (b) Kim, S. S.; Pauly, T. R.; Pinnavaia, T. J. *Chem. Commun.* **2000**, 1661. (c) Karkamkar, A.; Kim, S. S.; Pinnavaia, T. J. *Chem. Mater.* **2003**, 1661.

(20) (a) Feng, P.; Bu, X.; Pin, D. J. *Langmuir* **2000**, *16*, 5304. (b) Melosh, N. A.; Davidson, P.; Feng, P.; Pin, D. J.; Chmelka, B. F. *J. Am. Chem. Soc.* **2000**, *122*, 823. (c) Feng, P.; Bu, X.; Stucky, G. D.; Pin, D. J. *J. Am. Chem. Soc.* **2000**, *122*, 994.

(21) (a) Kruk, M.; Antochshuk, V.; Matos, J. R.; Jaroniec, M. *J. Am. Chem. Soc.* **2002**, *124*, 768. (b) Hunter, H. M. A.; Garcia-Bennett, A. E.; Shannon, I. J.; Zhou, W.; Wright, P. A. *J. Mater. Chem.* **2002**, *12*, 20. (c) Antochshuk, V.; Kruk, M.; Jaroniec, M. *J. Phys. Chem. B* **2003**, *107*, 11900.

(22) Newalkar, B. N.; Komarneni, S.; Turaga, U. T.; Katsuki, H. *J. Mater. Chem.* **2003**, *13*, 1710.

(23) (a) Liu, Y.; Pinnavaia, T. J. *J. Mater. Chem.* **2002**, *12*, 3179. (b) Liu, Y.; Pinnavaia, T. J. *Chem. Mater.* **2002**, *14*, 3. (c) Kim, S. S.; Zhang, W.; Pinnavaia, T. J. *Science* **1998**, *282*, 1302.

(24) (a) El-Safty, S. A.; Hanaoka, T. *Chem. Mater.* **2004**, *16*, 384. (b) El-Safty, S. A.; Hanaoka, T. *Adv. Mater.* **2003**, *15*, 1893.

(25) (a) Attard, G. S.; Glyde, J. C.; Göltner, C. G. *Nature* **1995**, *378*, 366. (b) Attard, G. S.; Edgar, M.; Göltner, C. G. *Acta Mater.* **1998**, *46*, 751.

(26) (a) Göltner, C. G.; Henke, S.; Weissenberger, M. C.; Antonietti, M. *Angew. Chem., Int. Ed.* **1998**, *37*, 613. (b) Göltner, C. G.; Berton, B.; Kramer, E.; Antonietti, M. *Adv. Mater.* **1999**, *11*, 395.

(27) (a) Jonsson, B.; Lindman, B.; Holmberg, K.; Kronberg, B. *Surfactants and Polymers in Aqueous Solution*; Wiley: Chichester, UK, 1998. (b) Alexandridis, P.; Andersson, K. *J. Phys. Chem. B* **1997**, *101*, 8103. (c) Goldmints, I.; Ga-er, Y.; Booth, C.; Smith, K. A.; Hatton, T. A. *Langmuir* **1999**, *15*, 1651. (d) Sakya, P.; Seddon, J. M.; Templer, R. H.; Mirkin, R. J.; Tiddy, G. J. T. *Langmuir* **1997**, *13*, 3706.

(28) (a) Alfredsson, V.; Anderson, M. W. *Chem. Mater.* **1996**, *8*, 1141. (b) Lui, X.; Tian, B.; Yu, C.; Gao, F.; Xie, S.; Tu, B.; Che, R.; Peng, L. M.; Zhao, D. *Angew. Chem., Int. Ed.* **2002**, *41*, 3876.

(29) Tian, B.; Liu, X.; Solovyov, L. A.; Liu, Z.; Yang, H.; Zhang, Z.; Xie, S.; Zhang, F.; Tu, B.; Yu, C.; Terasaki, O.; Zhao, D. *J. Am. Chem. Soc.* **2004**, *126*, 865.

(30) Sakamoto, Y.; Kaneda, M.; Terasaki, O.; Zhao, D. Y.; Kim. J. M.; Stucky, G. D.; Shin, H. J.; Ryoo, R. *Nature* **2000**, *408*, 449.

(31) (a) Liu, N.; Assink, R. A.; Smarsly, B.; Brinker, C. J. *Chem. Commun.* **2003**, 1146. (b) Yu, K.; Wu, X.; Brinker, C. J.; Ripmeester, J. *Langmuir* **2003**, *19*, 7282.

(32) (a) Kruk, M.; Jaroniec, M. *Chem. Mater.* **2003**, *15*, 2942. (b) Ravikovitch, P. I.; Neimark, A. V. *Langmuir* **2002**, *18*, 1550.

(33) The microemulsion liquid crystal mesophase systems were formulated by mixing the C_{12}-alkane (dodecane, $C_{12}H_{26}$) to F108 copolymer surfactants prior to the addition of the TMOS at each lyotropic phase domain to form a quaternary system (F108:dodecane:TMOS:H_2O). For all the syntheses of high order cage monoliths at F108/TMOS composition ratios of 70, 80, and 90 wt %, the ratio of F108 copolymer to dodecane was kept at 2:0.5.

(34) (a) Kruk, M.; Jaroniec, M.; Ko, C. H.; Ryoo, R. *Chem. Mater.* **2000**, *12*, 1961. (b) Ravikovitch, P. I.; Neimark, A. V. *J. Phys. Chem. B* **2001**, *105*, 6817.

(35) Yu, C.; Fan, J.; Tian, B.; Stucky, G. D.; Zhao, D. *J. Phys. Chem. B* **2003**, *107*, 13368.

(36) Smarsly, B.; Polarz, S.; Antonietti, M. *J. Phys. Chem. B* **2001**, *105*, 10473.

(37) (a) Mokaya, R. *Chem. Commun.* **2001**, 633. (b) Xia, Y.; Mokaya, R. *J. Mater. Chem.* **2004**, *14*, 2507. (c) Blin, J. L.; Leonard, A.; Su, B. L. *J. Phys. Chem. B* **2001**, *105*, 6070.

(38) Kruk, M.; Celer, E. B.; Jaroniec, M. *Chem. Mater.* **2004**, *16*, 698.

(39) El-Safty, S. A.; Hanaoka, T.; Mizukami, F. *Adv. Mater.* **2005**, *17*, 47.

(40) (a) Mokaya, R. *Angew. Chem., Int. Ed.* **1999**, *38*, 2930. (b) Pauly, T. R.; Petkov, V.; Billinge, S. J. L.; Pinnavaia, T. J. *J. Am. Chem. Soc.* **2002**, *124*, 97.

(41) (a) Chen, S. C.; Kawi, S. *J. Phys. Chem. B* **1999**, *103*, 8870. (b) Mokaya, R. *J. Phys. Chem. B* **2000**, *104*, 8279.